An Atomistic Model for Simulations of the General Anesthetic Isoflurane

Jérôme Hénin,*,†,⊥ Grace Brannigan,*,‡,⊥ William P. Dailey,§ Roderic Eckenhoff,|| and Michael L. Klein‡

Laboratoire d'Ingénierie des Systèmes Macromoléculaires, CNRS, Marseille, France, Institute for Computational Molecular Science and Department of Chemistry, Temple University, Philadelphia, Pennsylvania, Department of Chemistry, University of Pennsylvania, Philadelphia, Pennsylvania, and Department of Anesthesiology and Critical Care, University of Pennsylvania Medical Center, Philadelphia, Pennsylvania

Received: September 11, 2009; Revised Manuscript Received: October 28, 2009

An atomistic model of isoflurane is constructed and calibrated to describe its conformational preferences and intermolecular interactions. The model, which is compatible with the CHARMM force field for biomolecules, is based on target quantities including bulk liquid properties, molecular conformations, and local interactions with isolated water molecules. Reference data is obtained from tabulated thermodynamic properties and high-resolution structural information from gas-phase electron diffraction, as well as DFT calculations at the B3LYP level. The model is tested against experimentally known solvation properties in water and oil, and shows quantitative agreement. In particular, isoflurane is faithfully described as lipophilic, yet nonhydrophobic, a combination of properties critical to its pharmocological activity. Intermolecular interactions of the model are further probed through simulations of the binding of isoflurane to a binding site in horse spleen apoferritin (HSAF). The observed binding mode compares well with crystallographic data, and the calculated binding affinities are compatible with experimental results, although both computational and experimental measurements are challenging and provide results with limited precision. The model is expected to be useful for detailed simulations of the elementary molecular processes associated with anesthesia. Full parameters are provided as Supporting Information.

Introduction

Inhalation of certain volatile substances has been known to cause immobilization and loss of consciousness for more than a century, and use of compounds such as diethyl ether to perform anesthesia started what can be seen as a new era for surgery.[1] The major family of inhaled anesthetics historically available, and in part still used today, comprises halogenated alkanes (like halothane) and ethers, such as isoflurane. Despite being extensively used throughout the past century, the mechanism of general anesthesia by inhaled agents is hardly understood in any molecular detail.[2] Two types of mechanisms have been postulated to explain the modulation of synaptic transduction by anesthetics. Because of the correlation between anesthetic potency and oil/water partitioning coefficient known as the Meyer−Overton rule,[3,4] an indirect mechanism has been proposed, in which anesthetics affect response of the postsynaptic membrane by modulating its physical properties through interaction with its lipid component.[5] The other major research direction concerns direct interaction of general anesthetics with the ligand-gated ion channels that are responsible for the electrical response of the postsynaptic cell. Franks and Lieb observed[6] that Meyer−Overton-like solubility/potency correlation does not extend across *n*-alcohols and clinical anesthetics, although it can be improved if solubility in *n*-octanol, rather than olive oil, is considered. This led them to conclude that the sites of anesthetic action are not purely hydrophobic. The relevance of the Meyer−Overton rule was further brought into question by the discovery of *nonimmobilizers*,[7,8] lipophilic compounds (such as *n*-alkanes and halogenated alkanes) whose anesthetic potency is lower than would be expected from their oil solubility. Unlike alcohols, however, the anesthetic potency of these substances cannot be accounted for by a mere solubility rule in a simple solvent.[9,10] Pohorille and co-workers formulated a modified Meyer−Overton rule, stating that anesthetic potency correlates with preference toward polar/hydrophobic interfaces, rather than lipophilicity, and described anesthetic compounds as interfacially active.[10−14]

The broad, ongoing effort to investigate this mechanism in microscopic detail brings together experimental and computational approaches. Molecular modeling and simulations have been applied to the study of anesthetic partitioning into model membranes[11,12,15−17] as well as their interaction with transmembrane ion channels;[18−20] see ref 21 for a review. Simulation approaches require well-parametrized empirical models of the compounds involved. Compounds such as halothane and isoflurane are challenging in this respect, because few halogenated alkanes—and no halogenated ethers—are described by standard biomolecular force fields. Models of halothane were published by Scharf and Laasonen[22] and more recently by Tang and coworkers.[23] Those models were not designed for compatibility with biomolecular force fields, and thus may not yield an accurate description of the interactions of anesthetics with biomolecules. A recent modeling study by Bertaccini et al.[24] used a combined semiempirical/molecular mechanics description to model the polarization of halothane, dichloroethane, and

* To whom correspondence should be addressed. E-mail: jhenin@ifr88.cnrs-mrs.fr (J.H.); gbrannigan@temple.edu (G.B.).
† CNRS.
‡ Temple University.
§ University of Pennsylvania.
|| University of Pennsylvania Medical Center.
⊥ These authors contributed equally to this work.

10.1021/jp9088035 CCC: $40.75

bromoform in protein environments. Pohorille et al. constructed a model of isoflurane,[10] but the complete set of parameters was not published. Here, we present an empirical, atomistic model of isoflurane compatible with the widely used CHARMM force field for biomolecules,[25,26] and the water model TIP3P.[27] Target properties for the parametrization include the geometry, density, heat of vaporization, molecular electrostatic potential, and interaction with isolated water molecules. Additionally, the free energies of solvation in both water and oil are shown to agree quantitatively with experiment.

In order to verify that the isoflurane model interacts realistically with amphiphilic cavities like those to which it is thought to bind, interactions between isoflurane and HSAF were simulated. Ferritin is one of the few soluble proteins for which high-resolution structural data of a complex with an anesthetic is available. Ferritin monomers are four-helix bundles (similar in topology to the transmembrane domains of Cys-loop ligand-gated ion channel subunits); when oligomerized into the biological 24-mer, a small binding site with high affinity for anesthetics is formed at the interface between monomers.[28] Furthermore, measurement of binding affinity to the HSAF binding site can provide a preliminary screening process for the discovery of new anesthetics.[29] A previous[28] measurement of isoflurane affinity for HSAF used a racemic mixture; for a more direct comparison between simulation and experiment, we report on new experimental measurements, using enantiomerically pure isoflurane, indicating that (*S*)- and (*R*)-isoflurane have nearly equivalent affinities for HSAF. Computational binding affinity calculations of both enantiomers, as well as a relative affinity measurement, overlap experimental results within error.

Methods

The parametrization of isoflurane proceeded in stages, using target properties obtained either from our electronic structure calculations or the experimental literature. Published experimental values of condensed-phase properties (density and standard enthalpy of vaporization of liquid isoflurane,[30] and Gibbs free energy of solvation in water[31]) were used. Gas-phase properties were obtained from quantum mechanical calculations and include the minimum-energy structure, molecular electrostatic potential, and torsional potentials around C−C and C−O bonds, as well as the interaction energy and geometry of two isoflurane−water dimers. Electronic structure calculations were validated by comparison with high-resolution structural data obtained by gas-phase electron diffraction.[32]

Electronic Structure Calculations. All electronic structure calculations used the program Gaussian 03,[33] at the DFT level with the B3LYP hybrid exchange-correlation functional.[34,35] B3LYP is known to give accurate geometries for small molecules containing only first-row atoms[36] and to describe hydrogen-bonded complexes in good agreement with higher-level Møller−Plesset methods.[37] In isoflurane, the chlorine atom may not be as well-described by B3LYP as by less approximate methods, but the computational efficiency of B3LYP makes it attractive, and comparison with other data shows its accuracy to be sufficient (see the Results and Discussion section). A minimum-energy structure of (*S*)-isoflurane was obtained with a 6-311++G(2d,p) basis set. Fully relaxed potential energy surfaces (PESs) were computed for rotation around three torsional angles: F1−C1−C2−O, C1−C2−O−C3, and C2−C3−O−F4. Relaxed torsional scans in redundant internal coordinates used the 6-311G* basis set. To balance the nonbonded interactions with water, possible isoflurane−water complexes were optimized, although only two were found to be stable. In these calculations, all degrees of freedom were optimized with a counterpoise correction[38] to the basis set superposition error (BSSE) and tight convergence criteria; the basis set was 6-311+G(2d,p).

Parameter Adjustment. Reference values of bond length and valence angle parameters were taken from the minimum-energy conformer determined in the DFT calculation. Because the emphasis of this model is to describe accurately the conformations and intermolecular interactions of isoflurane, rather than its vibrational properties, force constants for those terms were taken to be typical values for similar structures in the CHARMM force field.

Torsional potentials, in contrast, were carefully fitted to reproduce the quantum-mechanical PES. Torsional terms of the CHARMM energy function have the form of cosine series:

$$V(\phi) = \sum_{k=1}^{n} V_k[1 + \cos(k\phi - \delta_k)] \qquad (1)$$

In the CHARMM force field, torsional potentials serve as corrections to purely nonbonded terms so that classical 1−4 interactions are consistent with quantum mechanical calculations. In principle, they could therefore be calculated by a nonlinear fit of expression 1 to the difference between the quantum-mechanical PES and the classical PES originating only from the nonbonded interactions. However, because of coupling through nonbonded interactions, the effective classical PES of each 1−4 interaction depends not just on the associated torsional parameter but on all torsional parameters in the molecule. Therefore, an iterative procedure was employed: each step determined an additional correction to the torsional parameters by performing a nonlinear fit of expression 1 to the difference between the quantum-mechanical PES and the classical PES determined using torsional parameters from the previous iteration.

Initial values of the Lennard-Jones (LJ) parameters were taken from those of related compounds in the CHARMM force field, refined based on bulk simulations and tested using solvation free energy calculations (see the corresponding Results and Discussion section below). An initial set of partial atomic charges was determined from a RESP calculation[39] with restrained hydrogen charges, based on the B3LYP/6-311+G(2d,p) molecular potential. A Mulliken population analysis gave unreasonably large charges. RESP charges were rounded to 0.01 *e* and only underwent a minor manual adjustment, as explained in the Results and Discussion section.

Charges and Lennard-Jones parameters were hand-modified to reproduce the stability, geometry, and energy of isoflurane−water complexes. The TIP3P water model[27] used with CHARMM predicts a water dimer interaction energy of −6.95 kcal/mol, larger than that predicted at the B3LYP level with BSSE correction (−4.84 kcal/mol). The target isoflurane−water interaction energies were scaled accordingly, in order to achieve a proper balance between water−solute and water−water interactions. This accounts for the fact that the force field is designed for the condensed phase rather than vacuum calculations: its parameters are adjusted to include a mean-field contribution of many-body polarization in the liquid phase.

The parametrization and testing process was iterated until a self-consistent set of torsional and nonbonded parameters was reached that satisfied all target properties. Because the CHARMM energy functional includes 1−4 nonbonded interactions, the conformation is very sensitive to nonbonded parameters, whereas bulk properties are not sensitive to minor changes in conformational properties. For that reason, the last step was a final adjustment of the torsional potentials.

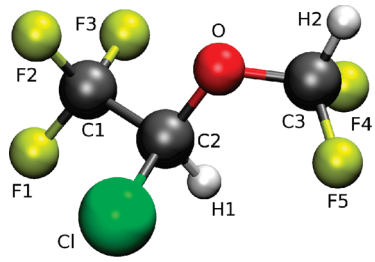

Figure 1. Ball-and-stick rendering of the minimum-energy structure of (*S*)-isoflurane, with labels indicating the atom naming convention. All molecular graphics were rendered using VMD.[40]

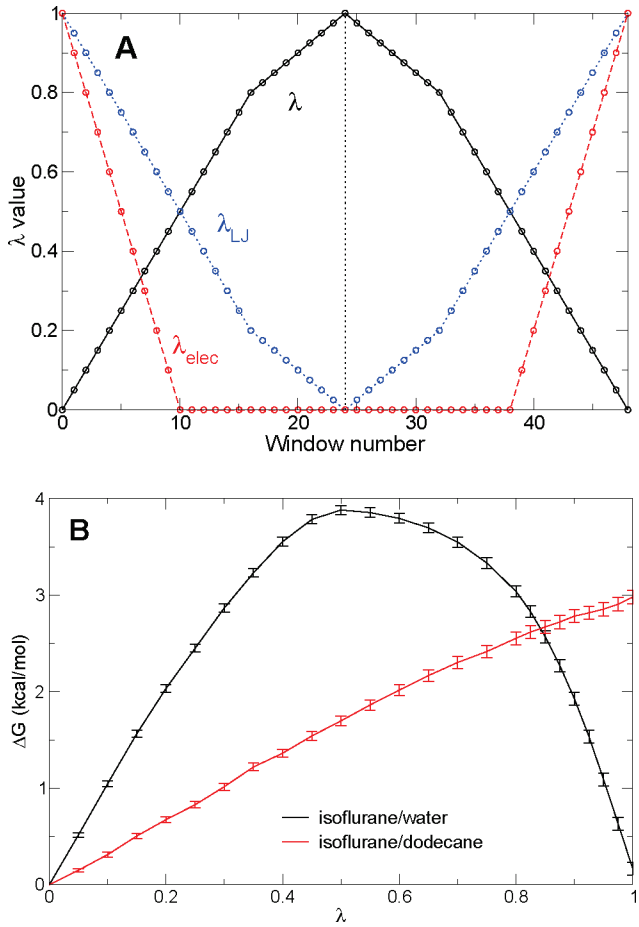

Figure 2. (A) Intermediate states for decoupling and recoupling isoflurane from its aqueous or organic solvent in solvation free energy calculations. Independent coupling parameters λ_{LJ} and λ_{elec} depend on the control parameter λ. (B) Computed free energy change as a function of decoupling parameter λ, for the isoflurane/water and isoflurane/dodecane systems. Error bars are calculated according to eq 8.

All terms of the potential energy function are inversion-symmetric, except for torsional potentials whose shift parameters δ_k are not 0 or 180°. Torsional parameters for (*R*)-isoflurane are derived from those of the (*S*) enantiomer by inverting the sign of the δ_k parameters. It should be noted that fluorine atoms F4 and F5, although chemically indistinguishable, play different roles in the present model due to the presence of a prochiral center at C3. The convention here is that F4 is in the pro-(*S*) position in (*S*)-isoflurane (as shown in Figure 1) and in the pro-(*R*) position in (*R*)-isoflurane.

Validation of Bulk Properties: Liquid Isoflurane Simulations. To calculate the density and heat of vaporization of pure isoflurane, molecular dynamics (MD) simulations of the bulk liquid were performed using the program NAMD.[41] A cubic periodic box containing 125 isoflurane molecules was simulated in the NPT ensemble at 298 K and 1 bar, using Langevin dynamics and the Langevin piston algorithm as implemented in NAMD.[42] Pairwise nonbonded interactions were truncated at a distance of 12 Å, with a smooth switching function above 10 Å. Full electrostatics were included through the particle mesh Ewald method, using a real-space grid spacing of 1 Å or less. The multiple time step r-RESPA integrator was used, with a base time step of 2 fs and an extended time step of 4 fs for soft, long-range interactions. For each set of parameters, a 100 ps equilibration (starting from a previously equilibrated liquid system) was followed by a 1 ns trajectory used to compute average properties.

Validation of Solvation Properties: Partition Coefficient in Water and Oil. Experiments measuring partitioning of anesthetics into nonpolar phases typically use olive oil, whose major components are triglycerides such as trioleoylglycerol. The bulk of the oil phase can hence be well described by long alkane chains: the present simulations use liquid dodecane as a nonpolar solvent. Solvation in water was studied using the modified TIP3P model[27] typically used with the CHARMM force field.

Solvation of isoflurane in both water and oil was studied along an unphysical, but computationally expedient pathway, wherein the solute is progressively decoupled from the solvent. Decoupling is obtained by turning off intermolecular interactions using a scaling parameter λ. These transformations were sampled using a modified version of the alchemical free energy feature of NAMD,[41] available with version 2.7b1[42] and later versions. This implementation performs a decoupling of the solute from its environment, where the nonbonded pair potential V_{NB} is scaled according to a dual coupling parameter (λ_{LJ}, λ_{elec}), and Lennard-Jones potentials are replaced with the soft-core potential of Zacharias et al.:[43]

$$V_{NB}(r_{ij}) = \lambda_{LJ}\varepsilon_{ij}\left[\left(\frac{R_{ij}^{\min 2}}{r_{ij}^2 + \delta(1-\lambda_{LJ})}\right)^6 - \left(\frac{R_{ij}^{\min 2}}{r_{ij}^2 + \delta(1-\lambda_{LJ})}\right)^3\right] + \lambda_{elec}\frac{q_i q_j}{\varepsilon_1 r_{ij}} \qquad (2)$$

where $R_{ij}^{\min}$ and ε_{ij} are the Lennard-Jones parameters of particle pair (i, j) (calculated from appropriate combination rules), q_i and q_j their respective charges, and the "shift distance" δ is a tunable parameter whose value affects the hardness of the soft-core potential for $0 < \lambda_{LJ} < 1$. In practice, λ_{elec} is scaled down to zero before λ_{LJ} reaches zero, thus avoiding the numerical singularities in the sampled interaction potential that would arise from bare charges.

As is common practice, the transformation was split into 24 stages or "windows", and run forward and backward (decoupling followed by recoupling), as indicated in Figure 2A. The "shift distance" parameter δ in eq 2 was set to 7.0 Å^2 for the water system and 5.5 Å^2 for the dodecane system, after optimization by trial-and-error. In each window, a short relaxation (1 ps) was followed by 25 ps of data collection. For each transformation, 10 independent simulations (replicas) were performed using different initial velocities and seeds for the stochastic term in the Langevin thermostat. The total simulation time for one transformation was 12.5 ns. The free energy change was computed using the simple overlap sampling (SOS) formula[44] based on data from all replicas, as explained in detail in the Appendix. This method is trivially parallel, even for a small system, and has excellent convergence properties provided that

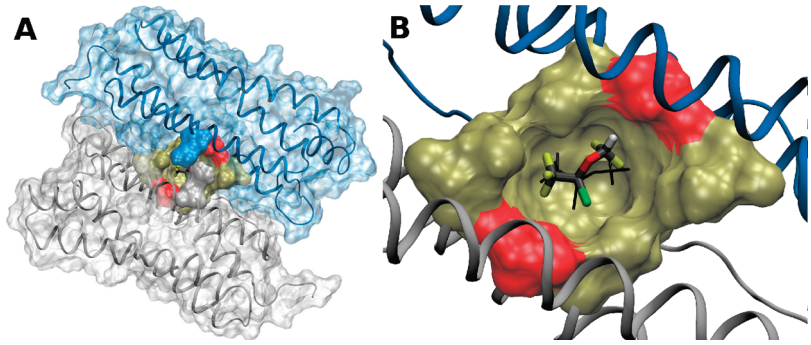

Figure 3. Position of isoflurane in the HSAF binding site. (A) The HSAF dimer from (PDB code 1XZ3) with the two L-chains shown in blue or silver. Main binding site residues are shown in tan and red, and the two Arg59 residues that form the gate to the binding site are in space-filling representation, also colored blue or silver. (B) Main binding site residues with hydrophobic residues in tan and polar residues in red (Arg59 not shown). The isoflurane orientation reported in 1XZ3 is illustrated with the black lines, and the isoflurane after energy minimization governed by the present model is shown in licorice.

relaxation of the system in response to a small change in the Hamiltonian is fast (small "Hamiltonian lag"[45]). In this case, it provides a larger number of decorrelated samples for each stage of the transformation than would a single run with an equivalent total sampling time. The method is ideally suited for solvation calculations such as the present ones.

The periodic aqueous system contained one isoflurane and 814 water molecules, forming a cubic box of water with a length of about 30 Å. The isoflurane/dodecane system contained 128 dodecane molecules in a cubic periodic box of length 36.6 Å. Dodecane was modeled by the CHARMM27 force field.[26] Simulations were run in the NPT ensemble, at a pressure of 1 bar and temperature of 298 K for water and 310 K for dodecane. Other simulation parameters were identical to those of pure isoflurane simulations.

The hydration free energy of isoflurane was also studied along a second, physical pathway, where one isoflurane molecule was transferred across a water−gas interface. This simulation was accelerated and the free energy profile computed using the NAMD implementation[46] of the adaptive biasing force method (ABF).[47,48] The ABF method relies on thermodynamic integration of the mean force exerted on a predefined collective variable to compute its associated free energy profile.

Transfer across the Water−Gas Interface. Transfer of isoflurane across a water−gas interface was simulated using the ABF method.[46−48] The periodic system contained a roughly cubic water lamella of length 30 Å. The z-dimension of the periodic box was 60 Å, leaving an empty space of the same size as the water lamella. The ABF algorithm was applied on the distance z between isoflurane and the center of the water lamella, projected onto the normal to the water−gas interface. The free energy derivative as a function of z was accumulated in 0.2 Å wide bins. Data was accumulated for a total simulation time of 120 ns.

Ferritin-Bound Isoflurane Simulations. Initial coordinates for MD simulations of one (*S*)-isoflurane molecule bound to apoferritin (Figure 3) were taken from crystallographic structure 1XZ3,[28] which reflects a crystal comprising only the HSAF light chain. The HSAF dimer was solvated in a rectangular box containing about 12 000 water molecules. Ions were added to neutralize the system and bring the ionic concentration to 0.1 M. The total number of atoms in the simulation box was about 40 000. The same setup was also used for a simulation of (*R*)-isoflurane: the (*S*) enantiomer was replaced with (*R*) and the C1−C3 pseudobonds were aligned.

Both systems were simulated using NAMD2.7b1 in the NPT ensemble, at pressure $P = 1$ bar and temperature $T = 300$ K. The simulations used the CHARMM22-CMAP force field with torsional cross-terms[49,50] for the protein, ion parameters from Beglov and Roux,[51] and the modified TIP3P water potential[27,52] (as in the solvation calculations). Periodic boundary conditions were applied, with particle mesh Ewald long-range electrostatics and a cutoff of 1.2 nm for Lennard-Jones potentials, with a smooth switching function starting at 1.0 nm. Bonds involving hydrogen atoms were constrained to their equilibrium length using the SHAKE/RATTLE algorithm. Multiple time step integration was carried out using r-RESPA, with a base time step of 2 fs and a secondary time step of 4 fs for long-range interactions. The NAMD2.7b1 collective variables module[42] was used to prevent rotation of the HSAF dimer within the simulation box, which would have caused interaction between periodic images, due to the dimer's oblong shape. Minimization for 100 steps was followed by 25 ns of production, over which the protein rmsd was stable.

Ferritin−Isoflurane Binding Free Energy Calculations. Binding affinity was calculated using the alchemical free energy perturbation (FEP) module of NAMD2.7b1. Three transformations were conducted: decoupling of (*S*)-isoflurane, decoupling of (*R*)-isoflurane, and mutation of (*S*) into (*R*). The final frame of the (*S*)-isoflurane/HSAF dimer equilibration simulation lasting 25 ns was used as the initial frame for the (*S*)-isoflurane decoupling and mutation calculations; the final frame of the (*R*)-isoflurane/HSAF dimer equilibration served as the initial frame for (*R*)-isoflurane decoupling. The two decoupling calculations included a restraint on the center of mass of the isoflurane molecule to prevent it from leaving the binding site while decoupled; the restraint exerted no force when the isoflurane center of mass was within 3.5 Å of the binding site center, and exerted a harmonic restoring force with a force constant of 5 kcal/mol/Å^2 when the center of mass was outside that range. In the mutation calculation, a harmonic restoring force with a constant of 5 kcal/mol/Å^2 was applied between the centers of mass of the (*S*)- and (*R*)-isoflurane molecules. The transformation was performed as successive decoupling (integration over λ from 0 to 1) and recoupling stages (integration over λ from 1 to 0). Each decoupling or recoupling stage was split into 22 windows, sampled for a total of 11 ns. For each system, a series of three successive decoupling and recoupling calculations were performed, or a total of 6 calculations and 66 ns of sampling. The (*S*)−(R) mutation was also sampled in six stages, i.e., three successive forward-and-backward transformations. Each stage was sampled for 12 ns, split uniformly between 24 windows; the total sampling time was 72 ns. There are two advantages to running the calculations forward and backward repeatedly: each

window is sampled with multiple initial conditions and the distribution of values across repeated simulations provides an estimate of the error in the calculation.

Experimental Measurements of Binding Affinity. The preparation of enantiomerically enriched samples of the isoflurane enantiomers followed the published procedure of Huang et al.[53] The final enantiomeric purity of the (*R*)-(−)-isoflurane sample was 96.9% ee, while that for the (*S*)-(+)-isoflurane sample was 44.2% ee. The lower value obtained for the (*S*) enantiomer was due to our difficulty in purifying the lower melting diastereomeric salt between (*R*)-(+)-dehydroabietylamine and (1-chloro-2,2,2-trifluoroethoxy)difluoroacetic acid. Values for enantiomeric purity were established using chiral gas chromatography on a 50 m Lipodex E capillary column operated at 30 C and 16 psi He.

Binding was measured using a fluorescence assay based on competition with 1-aminoanthracene (1-AMA) binding.[29] Briefly, various concentrations of (*R*)- and (*S*)-isoflurane were added to mixtures of HSAF (2 μM) and 1-AMA (4 μM) in phosphate-buffered saline, and fluorescence emission was measured at 510 nm with 380 nm excitation in filled, stoppered 0.5 mL quartz cuvettes. Emission of HSAF alone and of 1-AMA alone was subtracted from that of the mixture, and then plotted against the isoflurane concentration. Both (*R*)- and (*S*)-isoflurane experiments were conducted simultaneously to minimize systematic errors. Variable slope Hill curves were fitted to allow determination of IC_{50} and slope. IC_{50} values were converted to K_D values using the Cheng−Prusoff equation, and K_D values were converted to binding affinities using the following standard relationship

$$\Delta G_{bind} = -k_B T \ln K_A = k_B T \ln K_D \qquad (3)$$

where k_B is Boltzmann's constant, T is temperature, and the binding affinities $\Delta G^{(S)}_{bind}$ and $\Delta G^{(R)}_{bind}$ are reported in kcal/mol.

Results and Discussion

Molecular Conformations. Figure 1 shows the minimum-energy conformation of (*S*)-isoflurane, calculated at the B3LYP level. This optimized structure was compared to those determined by Hermann et al.,[32] using gas-phase electron diffraction (GED) and electronic structure calculations at the second-order Møller−Plesset (MP2) level of theory. In the following, structural parameters from GED are taken as a reference. The root-mean-square deviation (rmsd) from GED values of bond lengths is 0.009 Å for MP2 and 0.013 Å for our B3LYP calculation, while the uncertainty on GED data is 0.010 Å. Similarly, the rmsd from GED of valence angles is 0.92° for MP2 and 1.43° for B3LYP, with an uncertainty of 1.72° on GED data. Finally, the rmsd from GED for dihedral angles is 7.7° for MP2 and 6.6° for B3LYP with an uncertainty of 7.3° on GED values. It can hence be concluded that both the MP2 and B3LYP calculations agree with the very precise GED structural determination almost within its experimental uncertainty.

In the following, torsional angles C1−C2−O−C3 (ϕ_1) and C2−O−C3−H2 (ϕ_2) are used as conformational descriptors for isoflurane: conformers are labeled with their (ϕ_1, ϕ_2) pairs. In our calculations, the minimum-energy conformation is found to be the (*trans*, *trans*) conformer (−137, −179), very close to the result of Hermann et al. at the MP2 level (−136, −177).[32]

As important to this work as predicting the lowest-energy geometry is computing the relative energies of different conformations. Here, we take MP2 calculations by Herrman et al. as a reference. The B3LYP relative energy of the (*trans*, *gauche*$^-$) conformer, at 0.89 kcal/mol, is underestimated by 0.32 kcal/mol and that of the (*trans*, *gauche*$^+$) conformer, 2.58 kcal/mol, is underestimated by 0.49 kcal/mol. It is interesting to note that, in the same work, Hermann et al. present DFT calculations using the B3PW91 functional, which gives worse results (relative energies too low by 0.49 and 0.80 kcal/mol, respectively). Therefore, B3LYP seems to provide better energy accuracy than B3PW91 for isoflurane, at a similar cost—much lower than that of MP2.

TABLE 1: Torsional Parameters for (*S*)-Isoflurane

torsion	k	V_k (kcal/mol)	δ_k (deg)
F C_1 C_2 O	3	0.411	3
C_1 C_2 O C_3	1	0.654	6
	2	1.284	−87
	3	0.363	11
C_2 O C_3 F_4	1	−1.264	7
	2	0.656	−3
	3	0.603	4

Table 1 lists optimized torsional parameters. The resulting potential energy surfaces (PES) are shown in Figure 4, together with the quantum mechanically calculated targets. The combination of cosine series terms with independently fitted barrier heights (V_k) and phase factors (δ_k) with 1−4 nonbonded interactions allows for very faithful reproduction of the target energy landscape by the empirical model.

Bulk Properties and Isoflurane/Water Complexes. A trial set of Lennard-Jones parameters, based on CHARMM parameters for fluoroalkanes,[54] gave good results for bulk properties without further modification. The predicted density of the model at 298 K is 1.52 × 10^3 g/L, well within 2% of the experimental value of 1.50 × 10^3 g/L. Its enthalpy of vaporization is 7.6 kcal/mol, identical within experimental precision to the target value.[31]

Six putative isoflurane−water dimer structures were tested, each of which included a possible hydrogen bond (or weak, hydrogen-bond-like interaction). With one of the water hydrogens as well as the oxygen denoted as H_w and O_w, the six dimers tested were:

(1) H1−O_w
(2) H2−O_w
(3) O−H_w
(4) O−H_w, F4−H_w
(5) O−H_w, F5−H_w
(6) H1−O_w, F1−H_w, F2−H_w

Only the first two dimers were found to be stable at the B3LYP level—effectively forming weak C−H···O hydrogen bonds.[55]

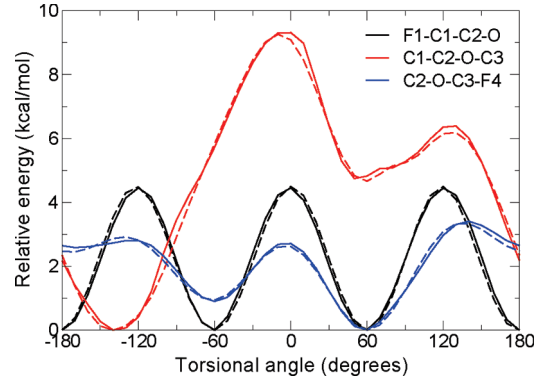

Figure 4. Ab initio and empirical potential energy surfaces for the torsional angles F1−C1−C2−O (black), C1−C2−O−C3 (red), and C2−O−C3−F4 (blue). Data is obtained from fully relaxed torsional scans at the B3LYP level (solid lines) and from the present model (dashed lines).

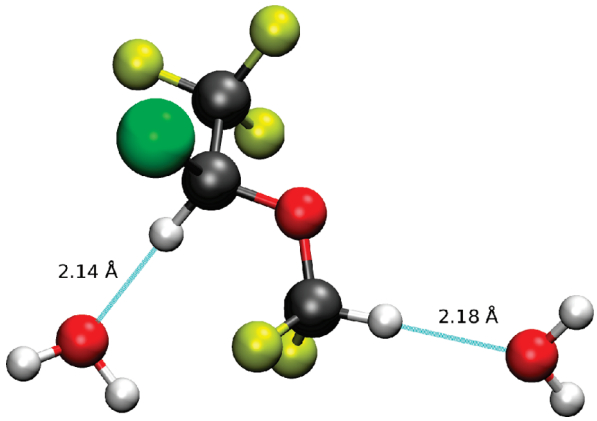

Figure 5. Isoflurane−water dimer structures. Rendering is similar to Figure 1. C−H···O hydrogen bonds are shown as dotted lines, with the hydrogen−oxygen distance. Isoflurane molecules from both dimers are aligned, but only one is shown—conformational variations in isoflurane are negligible.

TABLE 2: Nonbonded Parameters for Isoflurane: Partial Atomic Charges and Lennard-Jones Parameters (CHARMM Format)[a]

atom	charge (e)	(ref 10 charge)	ε (kcal/mol)	$R^{min}/2$ (Å)
C_1	0.38	0.683	−0.020	2.3
F_{1-3}	−0.11	−0.179	−0.097	1.6
C_2	−0.28	−0.413	−0.055	2.0373
H_1	0.25	0.287	−0.050	0.85
Cl	0.00	−0.028	−0.254	1.9811
O	−0.12	−0.111	−0.120	1.7
C_3	0.26	0.258	−0.042	2.05
F_{4-5}	−0.16	−0.141	−0.105	1.63
H_2	0.16	0.143	−0.050	0.84

[a] See Figure 1 for atom naming convention. Partial atomic charges from Pohorille et al.[10] are listed for comparison.

C−O distances for the two dimers are 3.23 and 3.27 Å, whereas the respective H−O distances are 2.14 and 2.18 Å. Optimized geometries are depicted in Figure 5. In the CHARMM force field, the difference between polar and nonpolar hydrogens largely stems from a more compact LJ radius, effectively resulting in stronger electrostatic interactions. Reproducing the stability and properties of the two dimers was achieved by manually tuning the partial charges of atoms C2 and H1 (transferring a charge of 0.03 e from H1 to C2), and adapting LJ parameters for the two hydrogen atoms. Final nonbonded parameters are listed in Table 2. The charge on CF3 fluorine atoms, −0.11, is slightly smaller than that in the CHARMM32 model for trifluoroethane (i.e., −0.15): This is explained by the presence of several additional electron withdrawing groups in the isoflurane molecule. The charge on the CF3 carbon, 0.38, is identical to CHARMM32. Overall, the present partial charges differ significantly from those proposed by Pohorille et al.[10] based on multiconfiguration ESP fitting, although direct comparison of partial charges is not warranted here because the LJ potentials also differ between the two models.

Partitioning into Water and Oil. Isoflurane can clearly be considered lipophilic, since its partition coefficient into oil at 310 K is 90.8,[31] corresponding to $\Delta G_{solv} = 2.8$ kcal/mol. It cannot, however, be considered hydrophobic because its water/gas partition coefficient is 1.08 at 298 K.[30] This corresponds to a standard solvation free energy of 5×10^{-2} kcal/mol, not significantly different from zero for most experimental and computational purposes. Indeed, this *lipophilic, yet nonhydrophobic* character is a key property differentiating between general anesthetics and nonimmobilizers: nonimmobilizers are both lipophilic and hydrophobic.[7,8]

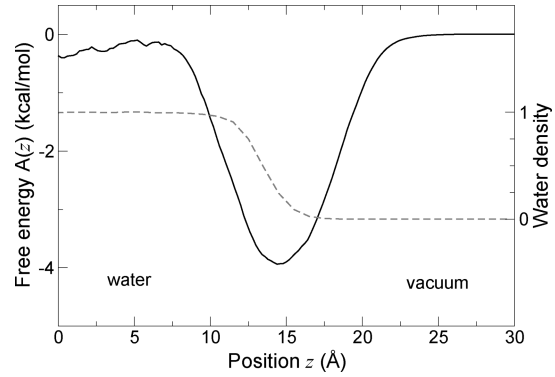

Figure 6. Free energy profile for the transfer of isoflurane across a water−vacuum interface (solid line). To locate the interface, water density is shown as a dashed line. Despite the lack of a preference for either bulk phase, isoflurane exhibits a strong tendency to populate the interface.

The results are presented in Figure 2B in the form of the free energy change as a function of the coupling parameter λ. The alchemical decoupling calculation gives a hydration free energy of -0.17 ± 0.07 kcal/mol, only a fraction of k_BT away from the experimental value. The free energy profile for the transfer of isoflurane across the water−gas interface is provided as Supporting Information. The net transfer free energy between the gas phase and bulk water agrees quantitatively with the alchemical decoupling result. Interestingly, isoflurane does exhibit a clear preference toward the interface, similar to its affinity for the polar/nonpolar interface as documented by Pohorille et al.[10] The solvation free energy in oil at 310 K is measured to be 3.0 ± 0.1 kcal/mol, again in good agreement with the experimental value of 2.8 kcal/mol. The complete decoupling free energy profile is provided as Supporting Information. Figure 6 depicts the free energy of transfer of isoflurane across the water−gas interface. The difference between plateau values agrees precisely with the partitioning free energy obtained from the alchemical decoupling calculation (Figure 2).

Binding to HSAF. ***Isoflurane Orientation.*** A racemic mixture of (*S*)- and (*R*)-isoflurane was used to measure the crystal structure of isoflurane bound to the HSAF dimer, but the resolution of the diffraction data was insufficient to distinguish between the two enantiomers.[28] Therefore, although the 1XZ3 structure is modeled with (*S*)-isoflurane only, the original density presumably contains some combination of (*S*) and (*R*). The isoflurane backbone (C1−C2−O−C3) comprises the most well-defined density, and it is possible that its orientation in the complex may be identical for both enantiomers. Therefore, the isoflurane orientation within the HSAF dimer binding site was defined by the orientation of the vector $\mathbf{r}$ joining atoms C_1 and C_3. The reference orientation was defined to reflect the symmetry of the binding site and depended upon $\mathbf{r_0}$, the (*S*)-isoflurane orientation in the crystal structure, and $\mathbf{r'_0}$, the orientation of its symmetry mate. The azimuthal angle θ was measured with respect to a z-axis defined as in Figure 7A, so that $\mathbf{r} = \mathbf{r_0}$ corresponded to an angle θ_0 and $\mathbf{r} = \mathbf{r'_0}$ corresponded to an angle $\theta'_0 = 180° - \theta_0$. The polar angle ϕ was measured with respect to the x-axis defined in Figure 7A, so that $\mathbf{r}$ corresponded to an angle ϕ_0 and $\mathbf{r'_0}$ corresponded to an angle $\phi'_0 = -\phi_0$. These definitions were used for both (*S*)- and (*R*)-isoflurane, based on the assumption that the C1−C3 vector had the same orientation for both enantiomers.

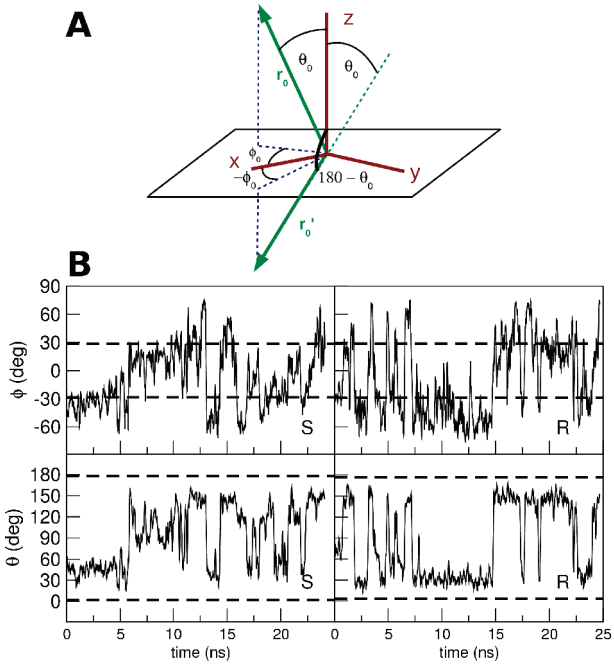

Figure 7. Orientation of isoflurane (measured according to the vector $\mathbf{r} = \mathbf{r}_{C1} - \mathbf{r}_{C3}$ in the HSAF binding site. (A) Definition of polar and azimuthal angles, with axes defined according to $\mathbf{r}_0$, the vector corresponding to isoflurane in the crystal structure 1XZ3, and $\mathbf{r}_0'$, the vector corresponding to its symmetry mate. (B) Evolution of ϕ and θ angles over the course of the MD simulation. The dashed lines represent the two symmetric orientations indicated by the crystal structure.

Evolution of the angles θ and ϕ throughout 25 ns of the MD simulation is shown in Figure 7 for both (*S*)- and (*R*)-isoflurane. Both switch between two equivalent well-defined orientations that correspond reasonably well with those measured in the crystal structure. The difference between a typical configuration at $\theta = 30°$ as observed in the simulation and the crystal structure is shown in Figure 3B. (*S*)-isoflurane, however, does transiently occupy a third orientation ($\theta = 90°$) perpendicular to that observed experimentally; this orientation corresponds to isoflurane pointing its difluoromethyl group out the opening of the binding site and hydrogen bonding with nearby water.

The binding free energies $\Delta G_{\text{bind}}^{(S)}$ and $\Delta G_{\text{bind}}^{(R)}$ for the *S* and *R* isomer, respectively, are computed from simulations as

$$\Delta G_{\text{bind}}^{(S)} \equiv -(\Delta G_{\text{u}}^{(S)} + \Delta G_{\text{hyd}}) = -(\Delta G_{\text{r}}^{(S)} + \Delta G_{\text{hyd}} + \Delta G_{\text{restr}})$$

$$\Delta G_{\text{bind}}^{(R)} \equiv -(\Delta G_{\text{u}}^{(R)} + \Delta G_{\text{hyd}}) = -(\Delta G_{\text{r}}^{(R)} + \Delta G_{\text{hyd}} + \Delta G_{\text{restr}}) \quad (4)$$

where the components of ΔG_{bind} are defined in Scheme 1: $\Delta G_{\text{r}}^{(R)}$ and $\Delta G_{\text{r}}^{(S)}$ correspond to decoupling of isoflurane from the HSAF binding site, with a center-of-mass restraint imposed to keep the isoflurane molecule in the binding site, and is calculated using FEP. ΔG_{hyd} correponds to the solvation free energy of isoflurane, as reported in the previous section. ΔG_{restr} is the translational entropy cost of imposing the restraint, equivalent to

$$\Delta G_{\text{restr}} = k_{\text{B}} T \ln\left(\frac{V}{V^*}\right) \quad (5)$$

where V is the volume of the spherical region of radius $r_{\text{restr}} =$ 3.5 Å forming the flat portion of the restraint and V^* is the volume available to one isoflurane molecule in a 1 M solution (the standard state).

SCHEME 1: Thermodynamic Cycle for Measurement of (*S*)- and (*R*)- Isoflurane Binding Affinities[a]

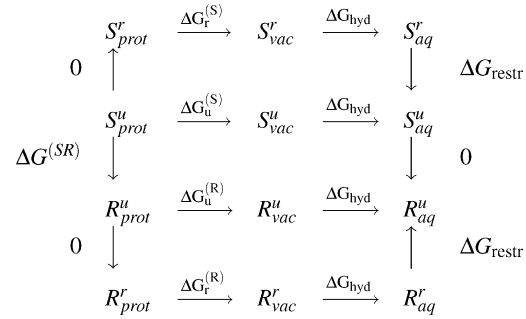

[a] "r" and "u" superscripts refer to restrained and unrestrained, respectively, while "prot", "vac", and "aq" subscripts refer to the ligand environment: protein, vacuum, or aqueous. Binding affinities are described by eq 4.

TABLE 3: Values Corresponding to the Free Energy Changes Defined in Scheme 1, as Measured Using Free Energy Perturbation[a]

quantity	SOS (kcal/mol)	range (kcal/mol)	Expt (kcal/mol)
$\Delta G_{\text{c}}^{(S)}$	9.3	8.0 to 10.7	
$\Delta G_{\text{c}}^{(R)}$	10.3	9.5 to 11.1	
ΔG_{hyd}	-0.2 ± 0.1[b]	−0.4 to 0.1	0.05[c]
ΔG_{restr}	−1.3[d]		
$\Delta G^{(SR)}$	0.1	−0.4 to 0.8	0.1[e]
$\Delta G_{\text{bind}}^{(S)}$	−7.8	−6.5 to −9.2	−5.4,[f] −6.0,[g] −7.3[h]
$\Delta G_{\text{bind}}^{(R)}$	−8.8	−8.0 to −9.6	−5.3,[f] −6.0,[g] −7.3[h]

[a] ΔG_{restr} is calculated via eq 5, and $\Delta G_{\text{bind}}^{(S)}$ and $\Delta G_{\text{bind}}^{(R)}$ are calculated via eq 4. [b] Error margin calculated from eq 8. [c] Reference 30. [d] Equation 5. [e] The difference of $\Delta G_{\text{bind}}^{(S)}$ and $\Delta G_{\text{bind}}^{(R)}$ as reported here. [f] Present measurements using competition of enantiomer-enriched isoflurane with 1-AMA. [g] Low affinity site measured using ITC and a racemic mixture.[28] [h] High affinity site measured using ITC and a racemic mixture.[28]

Binding Affinity. Experimentally, both (*R*)- and (*S*)-isoflurane reduced the fluorescence emission from the HSAF/1-AMA mixture essentially identically in a concentration-dependent manner. Final values of $\Delta G_{\text{bind}}^{(S)}$ and $\Delta G_{\text{bind}}^{(R)}$ are separated by less than 0.1 kcal/mol, as reported in Table 3. These values compare well with previous measurements[28,29] using the racemic mixture and either competitive binding with 1-AMA or ITC. In ref 28, however, ITC data was best fit by a two-site model with two sites of different affinity; this result was interpreted to indicate either enantiomerically sensitive affinities or different affinities to sites formed by two light chains compared to a light and heavy chain. Combined with data from the competition assay, experiments suggest a binding affinity ranging from −5.3 to −7.3 kcal/mol.

Final computational results for $\Delta G_{\text{bind}}^{(S)}$ and $\Delta G_{\text{bind}}^{(R)}$ are compared to experimental results in Table 3; the progress of the calculations as a function of λ is shown in Figure 8. Over the course of the calculation, the protein undergoes structural changes due in part to the decoupling algorithm and in part due to natural fluctuations. In particular, Arg59 in the HSAF dimer binding site fluctuates between multiple possible conformations that would require over 100 ns of simulation per window to sample fully; for 22 windows, this corresponds to at least 2.2 μs per calculation. Over shorter, more feasible time scales, it is possible that Arg59 will be in two different conformations in windows $\lambda = 0$ and $\lambda = 1$, due to fluctuations rather than the difference in λ. The difference in free energy between these two conformations will still be included in the

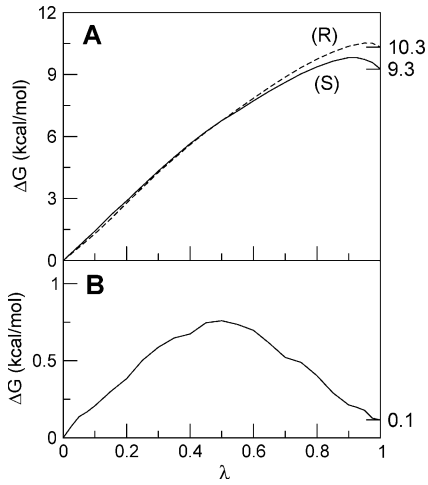

Figure 8. (A) Computed free energy change as a function of decoupling parameter λ, for the (*S*)-isoflurane/HSAF (solid line) and (*R*)-isoflurane/HSAF (dashed line) systems. (B) Computed free energy change as a function of mutation parameter λ, for mutation of (*S*) into (*R*)-isoflurane.

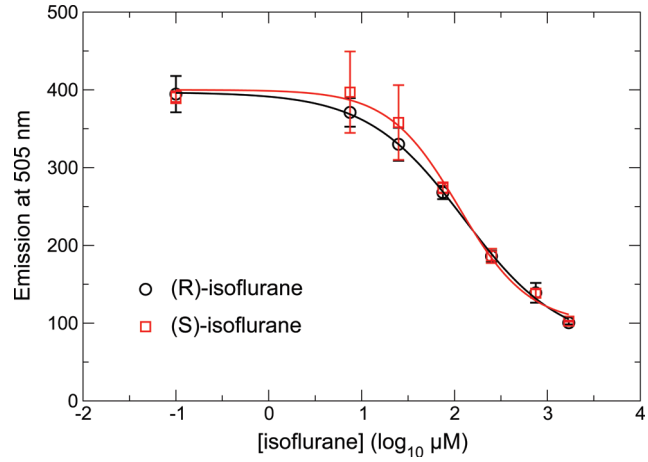

Figure 9. Fluorescence competition. The HSAF concentration was 1.2 mg/mL (2 μM), and the 1-AMA was 4 μM. Each point represents two independent experiments, and the Hill curve R^2 was 0.99 in both cases. IC_{50} values (in μM with 95% CI) for (*R*) were 126 (107−149) and for (*S*) were 111 (89−138). Hill slopes were not different: 0.83 for (*R*) and 1.14 for (*S*)-isoflurane.

total decoupling free energy, resulting in an error in the estimated binding affinity.

Such error can be reduced and its extent characterized by using multiple coupling and decoupling cycles per calculation, as described in the Methods section. In this approach, multiple homologous windows are sampled for each value of λ, but each is separated by a certain amount of time in which the protein has been allowed to evolve. The separate but identical windows will therefore sample a wider range of conformational space. The distribution of FEP values for repeated transformations provides an estimate of the error caused by slow fluctuations of the protein. The range of the data, rather than a standard error, is provided in Table 3 because the distributions are unlikely to be normal, and successive cycles may not be fully decorrelated.

The SOS column of Table 3 reflects one standard overlap sampling calculation involving all six stages (three coupling and three decoupling) of the data; such an analysis yields $\Delta G^{(S)}_{\text{bind}} = -7.8$ kcal/mol and $\Delta G^{(R)}_{\text{bind}} = -8.8$ kcal/mol. The distributions of experimental and computational measurements overlap for $\Delta G^{(S)}_{\text{bind}}$ but are separated by at least 0.7 kcal/mol for $\Delta G^{(R)}_{\text{bind}}$. Mutation of (*S*) into (*R*) within the HSAF dimer binding site, however, suggests that $\Delta G^{(SR)}_{\text{bind}} \equiv \Delta G^{(R)}_{\text{bind}} - \Delta G^{(S)}_{\text{bind}} = 0.1$ kcal/mol, in agreement with experimental results and the overlapping distributions of the (*S*)- and (*R*)-isoflurane decoupling calculations but inconsistent with the difference in the mean of the distributions. This inconsistency highlights the difficulties involved in computationally obtaining binding affinities to sites with slow dynamics, and further indicates that the calculations are only accurate within 1−2 kcal/mol. Differences between experimental and computational results may also be introduced by the presence of a heavy chain in the experimental measurements that was absent from the calculations. In summary, the present isoflurane model provides agreement with experimental measurements of binding affinity to HSAF within the limitations of both methods.

Conclusion

An atomistic model of isoflurane has been calibrated to faithfully describe its conformational preferences and intermolecular interactions. Targets for the parametrization include the complete gas-phase conformational energy surface, the molecular electrostatic potential and weak hydrogen bonding to individual water molecules, as well as the density and enthalpy of vaporization of the pure liquid. Isoflurane is found to form weak yet significant hydrogen bonds with water and other hydrogen acceptors. When combined with the CHARMM force field and TIP3P water, the model reproduces experimental solvation data in both water and oil, as indicated by precise free energy calculations. Therefore, the model is expected to provide an accurate description of the behavior of isoflurane at polar/nonpolar interfaces and in amphiphilic sites, which have been suggested to be important for anesthetic action.[6,10−14]

The calculated binding affinity of isoflurane to the HSAF binding site agrees with the experimental value, within estimated error. Furthermore, simulations are able to reproduce the orientation of HSAF-bound isoflurane found in the crystal structure. These results support the validity of the isoflurane model for use with proteins described by the CHARMM force field. Simulations are presently underway to investigate the interactions of isoflurane with both membrane lipids and protein cavities.

Acknowledgment. The authors are grateful to Floris Buelens, Peter Freddolino, and Chris Harrison for sharing and helping with preproduction software, and to Guillaume Lamoureux for helpful discussions. This work was supported by the National Institutes of Health through grant GM055876 and by the National Science Foundation through TeraGrid resources provided by the National Institute for Computational Sciences.

Appendix: Simple Overlap Sampling over Multiple Replicas

This section presents the expressions used to compute a free energy change ΔA using the simple overlap sampling (SOS) formula described by Lu et al.,[44] based on multiple, independent simulations (replicas). In this simple scheme, there is no interaction between replicas: their only role is to provide independent sampling.

We consider an "alchemical" transformation between two states, broken up into n stages or windows by defining a series of $n - 1$ intermediate states. Each of the states i is characterized by the potential energy function $E_i(\vec{r})$. R replica simulations are

performed, each of them sampling the forward and backward transformations.

For the forward transformation of window i in replica j, we define

$$x_{ij}^{(f)} = \langle e^{-\beta\Delta E_i/2}\rangle_{ij}^{(f)} \quad \text{and} \quad x_{ij}^{(b)} = \langle e^{-\beta\Delta E_i/2}\rangle_{ij}^{(b)} \qquad (6)$$

where $\Delta E_i = E_{i+1} - E_i$ and the superscripts f and b indicate sampling of the forward or backward transformation, respectively.

The averages over all replicas are defined as

$$\bar{x}_i^{(f)} = \frac{1}{R}\sum_{j=1}^{R} x_{ij}^{(f)} \quad \text{and} \quad \bar{x}_i^{(b)} = \frac{1}{R}\sum_{j=1}^{R} x_{ij}^{(b)}$$

with standard errors (assuming independent replicas):

$$\varepsilon^2(\bar{x}_i^{(f)}) = \frac{1}{R^2}\sum_{j=1}^{R}(x_{ij}^{(f)})^2 - \frac{1}{R}(\bar{x}_i^{(f)})^2 \quad \text{and} \quad \varepsilon^2(\bar{x}_i^{(b)}) = \frac{1}{R^2}\sum_{j=1}^{R}(x_{ij}^{(b)})^2 - \frac{1}{R}(\bar{x}_i^{(b)})^2$$

where R is the number of replicas. Then, the SOS expression for the free energy change in one window is simply[44]

$$e^{-\beta\Delta A_i} = \frac{\bar{x}_i^{(f)}}{\bar{x}_i^{(b)}}$$

and the total free energy change is

$$\Delta A = -\frac{1}{\beta}\sum_{i=1}^{n} \ln\left(\frac{\bar{x}_i^{(f)}}{\bar{x}_i^{(b)}}\right) \qquad (7)$$

The standard error of the estimator of ΔA given in eq 7 can then be estimated as

$$\varepsilon(\Delta A) = \frac{1}{\beta}\left[\sum_{i=1}^{n}\left(\frac{\varepsilon(\bar{x}_i^{(f)})}{\bar{x}_i^{(f)}}\right)^2 + \left(\frac{\varepsilon(\bar{x}_i^{(b)})}{\bar{x}_i^{(b)}}\right)^2\right]^{1/2} \qquad (8)$$

Supporting Information Available: CHARMM-format topology and parameter files and PDB coordinate files for (*S*)- and (*R*)-isoflurane. This material is available free of charge via the Internet at http://pubs.acs.org.

References and Notes

(1) Long, C. W. *South. Med. Surg. J.* **1849**, *5*, 705–713.
(2) Eckenhoff, R. G. *Mol. Interventions* **2001**, *1*, 258–268.
(3) Meyer, H. H. *Arch. Exp. Pathol. Pharmakol.* **1899**, *42*, 109–118.
(4) Overton, C. E. *Studien über die Narkose, zugleich ein Beitrag zur allgemeinen Pharmakologie*; Gustav Fischer Verlag: Jena, Germany, 1901.
(5) Cantor, R. S. *Biochemistry* **1997**, *36*, 2339–2344.
(6) Franks, N. P.; Lieb, W. R. *Nature* **1978**, *274*, 339–342.
(7) Taheri, S.; Laster, M. J.; Liu, J.; Eger, E. I.; Halsey, M. J.; Koblin, D. D. *Anesth. Analg.* **1993**, *77*, 7–11.
(8) Koblin, D. D.; Chortkoff, B. S.; Laster, M. J.; Eger, E. I.; Halsey, M. J.; Ionescu, P. *Anesth. Analg.* **1994**, *79*, 1043–1048.
(9) Fang, Z.; Ionescu, P.; Chortkoff, B. S.; Kandel, L.; Sonner, J.; Laster, M. J.; Eger, E. I. *Anesth. Analg.* **1997**, *84*, 1042–1048.
(10) Pohorille, A.; Wilson, M. A.; Chipot, C. *Prog. Colloid Polym. Sci.* **1997**, *103*, 29–40.
(11) Pohorille, A.; Cieplak, P.; Wilson, M. A. *Chem. Phys.* **1996**, *204*, 337–345.
(12) Chipot, C.; Wilson, M. A.; Pohorille, A. *J. Phys. Chem. B* **1997**, *101*, 782–791.
(13) Eger, E. I.; Koblin, D. D.; Harris, R. A.; Kendig, J. J.; Pohorille, A.; Halsey, M. J.; Trudell, J. R. *Anesth. Analg.* **1997**, *84*, 915–918.
(14) Pohorille, A.; Wilson, M. A.; New, M. H.; Chipot, C. *Toxicol. Lett.* **1998**, *100−101*, 421–430.
(15) Tu, K.; Tarek, M.; Klein, M. L.; Scharf, D. *Biophys. J.* **1998**, *75*, 2123–2134.
(16) Koubi, L.; Tarek, M.; Klein, M. L.; Scharf, D. *Biophys. J.* **2000**, *78*, 800–811.
(17) Vemparala, S.; Saiz, L.; Eckenhoff, R. G.; Klein, M. L. *Biophys. J.* **2006**, *91*, 2815–2825.
(18) Tang, P.; Xu, Y. *Proc. Natl. Acad. Sci. U.S.A.* **2002**, *99*, 16035–16040.
(19) Tang, P.; Mandal, P. K.; Zegarra, M. *Biophys. J.* **2002**, *83*, 1413–1420.
(20) Vemparala, S.; Domene, C.; Klein, M. L. *Biophys. J.* **2008**, *94*, 4260–4269.
(21) Trudell, J. R.; Bertaccini, E. *Br. J. Anaesth* **2002**, *89*, 32–40.
(22) Scharf, D.; Laasonen, K. *Chem. Phys. Lett.* **1996**, *258*, 276–282.
(23) Liu, Z.; Xu, Y.; Saladino, A. C.; Wymore, T.; Tang, P. *J. Phys. Chem. A* **2004**, *108*, 781–786.
(24) Bertaccini, E. J.; Trudell, J. R.; Franks, N. P. *Anesth. Analg.* **2007**, *104*, 318–324.
(25) MacKerell, A. D.; et al. *J. Phys. Chem. B* **1998**, *102*, 3586–3616.
(26) Feller, S. E.; MacKerell, A. D., Jr. *J. Phys. Chem. B* **2000**, *104*, 7510–7515.
(27) Jorgensen, W. L.; Chandrasekhar, J.; Madura, J. D.; Impey, R. W.; Klein, M. L. *J. Chem. Phys.* **1983**, *79*, 926–935.
(28) Liu, R.; Loll, P. J.; Eckenhoff, R. G. *FASEB J.* **2005**, *19*, 567–576.
(29) Butts, C. A.; Xi, J.; Brannigan, G.; Saad, A. A.; Venkatachalan, S. P.; Pearce, R. A.; Klein, M. L.; Eckenhoff, R. G.; Dmochowski, I. J. *Proc. Natl. Acad. Sci. U.S.A.* **2009**, *106*, 6501–6506.
(30) Smith, R. A.; Porter, E. G.; Miller, K. W. *Biochim. Biophys. Acta* **1981**, *645*, 327–338.
(31) FDA drug information for Forane (isoflurane); Baxter Healthcare Corporation, 2006.
(32) Hermann, A.; Mack, H.-G.; Oberhammer, H. *J. Fluorine Chem.* **2000**, *101*, 223–231.
(33) Frisch, M. J.; et al. *Gaussian 03*, revision B.04; Gaussian, Inc.: Wallingford, CT, 2004.
(34) Becke, A. D. *J. Chem. Phys.* **1993**, *98*, 5648.
(35) Lee, C.; Yang, W.; Parr, R. *Phys. Rev. B.* **1988**, *37*, 785–789.
(36) Ma, B.; Lii, J.-H.; Schaefer, H. F., III; Allinger, N. L. *J. Phys. Chem.* **1996**, *100*, 8763–8769.
(37) Lozynski, M.; Rusinska-Roszak, D.; Mack, H.-G. *J. Phys. Chem. A* **1998**, *102*, 2899–2903.
(38) Simon, S.; Duran, M.; Dannenberg, J. J. *J. Chem. Phys.* **1996**, *105*, 11024.
(39) Bayly, C. I.; Cieplak, P.; Cornell, W. D.; Kollman, P. A. *J. Phys. Chem.* **1993**, *97*, 10269–10280.
(40) Humphrey, W.; Dalke, A.; Schulten, K. *J. Mol. Graphics* **1996**, *14*, 33–38, 27−28.
(41) Phillips, J. C.; Braun, R.; Wang, W.; Gumbart, J.; Tajkhorshid, E.; Villa, E.; Chipot, C.; Skeel, R. D; Kalé, L.; Schulten, K. *J. Comput. Chem.* **2005**, *26*, 1781–1802.
(42) Bhandarkar, M.; et al. *NAMD user's guide*, version 2.7; Theoretical biophysics group, University of Illinois and Beckman Institute: Urbana, IL, 2008.
(43) Zacharias, M.; Straatsma, T. P.; McCammon, J. A. *J. Chem. Phys.* **1994**, *100*, 9025–9031.
(44) Lu, N.; Singh, J. K.; Kofke, D. A. *J. Chem. Phys.* **2003**, *118*, 2977–2984.
(45) Wood, R. H. *J. Phys. Chem.* **1991**, *95*, 4838–4842.
(46) Hénin, J.; Chipot, C. *J. Chem. Phys.* **2004**, *121*, 2904–2914.
(47) Darve, E.; Pohorille, A. *J. Chem. Phys.* **2001**, *115*, 9169–9183.
(48) Darve, E.; Rodríguez-Gómez, D.; Pohorille, A. *J. Chem. Phys.* **2008**, *128*, 144120.
(49) MacKerell, A. D., Jr.; et al. *J. Phys. Chem. B* **1998**, *102*, 3586–3616.
(50) MacKerell, A. D.; Feig, M.; Brooks, C. L. *J. Am. Chem. Soc.* **2004**, *126*, 698–699.
(51) Beglov, D.; Roux, B. *J. Chem. Phys.* **1994**, *100*, 9050–9063.
(52) Brooks, B. R.; Bruccoleri, R. E.; Olafson, B. D.; States, D. J.; Swaminathan, S.; Karplus, M. *J. Comput. Chem.* **1983**, *4*, 187–217.
(53) Huang, C. G.; Rozov, L. A.; Halpern, D. F.; Vernice, G. G. *J. Org. Chem.* **1993**, *58*, 7382–7387.
(54) Chen, I. J.; Yin, D.; MacKerell, A. D. *J. Comput. Chem.* **2002**, *23*, 199–213.
(55) Green, R. D. *Hydrogen Bonding by C-H Groups*; Wiley Interscience: New York, 1974.

JP9088035